JrnlID 10008_ArtID 4622_Proof# 1 - 18/05/2020

Journal of Solid State Electrochemistry
https://doi.org/10.1007/s10008-020-04622-1

ORIGINAL PAPER

Effect of supporting electrolyte concentration on one-step electrodeposited $CuInS_2$ films for ZnS/$CuInS_2$ solar cell applications

C. A. Rodríguez[1,2] · A. Delgadillo[2] · J. Nuñez[3] · G. Cabello-Guzmán[4] · Adriana C. Mera[1,2] · M. P. Delplancke[5] · B. Villacampa[6] · C. Carrasco[3]

Received: 26 February 2020 / Revised: 23 April 2020 / Accepted: 24 April 2020

Abstract

A one-step electrodeposition process was used to obtain $CuInS_2$ (CIS) films on a molybdenum substrate by varying the supporting electrolyte (lithium chloride, LiCl) concentration. The as-deposited samples were characterized by scanning electron microscopy, energy-dispersive spectroscopy, profilometry, and diffuse reflectance spectroscopy. From characterization, it was found that different concentrations of LiCl mainly lead to a morphological change in the obtained CIS films. Moreover, their chemical composition shifted to the stoichiometric composition for high concentrations of the supporting electrolyte. After annealing, the structural analysis from X-ray diffraction revealed that all samples crystallized in the tetragonal phase of CIS. In addition, it was found that the crystallite size increased for samples grown at higher concentrations of LiCl. Optical studies carried out by diffuse reflectance spectroscopy revealed that the band gap values increased from ~ 1.40 to ~ 1.45 eV (average) after the annealing process. Finally, zinc sulfide (ZnS) thin films were chemically deposited onto electrodeposited CIS films in order to evaluate the photovoltaic response of ZnS/CIS bilayer systems. We discovered that ZnS thin films covered the surface of CIS more effectively for the highest concentration of LiCl and that only the ZnS/CIS bilayer with the CIS film obtained at the highest concentration of LiCl showed a photovoltaic response.

Q2 **Keywords** $CuInS_2$ films · Electrodeposition · Electrolyte · Thin-film solar cells

Introduction

$CuInS_2$ (CIS) is a ternary semiconductor with excellent potential as an absorbent material for thin-film solar cells (TFSCs) [1–5]. Experimentally, CIS-based solar cells exhibit a limited energy conversion efficiency when compared with other chalcopyrite ternary semiconductor–based photovoltaic devices, such as $CuXSe_2$ (X = In or Ga) and $Cu(In,Ga)Se_2$ [6, 7]. However, the low cost and toxicity of CIS make it a promising candidate as an absorbent layer in solar cells.

Although the highest efficiency currently achieved for CIS-based solar cells is of only 13% [8], there is still potential to increase the conversion efficiency based on the optical properties of the material and its theoretical energy conversion efficiency of 32% [9]. CIS has a direct band gap of ~ 1.5 eV and a high absorption coefficient (10^5 cm^{-1}), which ensures absorption of most of the visible solar spectrum [10, 11]. This compound has good radiation stability and environmental compatibility, which should allow CIS photovoltaic devices to maintain performance even in adverse conditions [12].

✉ C. A. Rodríguez
arodriguez@userena.cl

Q1
1 Multidisciplinary Research Institute for Science and Technology, Universidad de La Serena, 1015 Juan Cisternas Av, La Serena, Chile

2 Department of Chemistry, Faculty of Sciences, University of La Serena, Campus Andrés Bello, 1305 Raúl Bitrán Av., La Serena, Chile

3 Thin Films and Electrochemical Process Laboratory, Departamento de Ingeniería de Materiales, Universidad de Concepción, Edmundo Larenas, 270 Concepción, Chile

4 Department of Basic Sciences, Faculty of Sciences, University of Bío-Bío, Campus Fernando May, Chillán, Chile

5 4MAT, Université Libre de Bruxelles, 50 Roosevelt Av., CP 165/63, 1050 Brussels, Belgium

6 Department of Condensed Matter Physics, ICMA, Universidad de Zaragoza-CSIC, 50009 Zaragoza, Spain

So far, several methods, such as co-evaporation, sputtering, spray pyrolysis, and electrodeposition, have been used for the fabrication of CIS thin films [13–15]. Among these methods, co-evaporation and sputtering are the most used to synthesize CIS films for TFSC applications. However, expensive equipment is needed for vacuum environments and high purity targets must be used in these deposition techniques. Therefore, these two methods are expensive for the production of large-area CIS thin films. In contrast, electrodeposition is an attractive method that can be used to fabricate large-area thin films at a lower cost.

Currently, there are two routes for the electrodeposition of CIS: one- and two-step routes [10, 16, 17]. In the two-step route, a layer of Cu-In is followed by a thermal sulfurization process to form CIS. In the one-step route, a sulfur source (commonly sodium thiosulfate) with metallic copper and indium ions are deposited simultaneously on the substrate surface. Accordingly, in the two-step route, the procedure becomes more complicated and the subsequent sulfurization process at high temperature requires the usage of a H_2S or S atmosphere, which are harmful, corrosive, and flammable [2, 18]. Since greener fabrication processes are increasingly required, efforts to exclude H_2S throughout the synthesis of semiconductor thin films have to be utilized [2, 19, 20]. Thus, the one-step electrodeposition process has arisen as a less toxic, simpler, and cheaper route to fabricate large-area CIS thin films.

The effect of different experimental conditions on the one-step electrodeposition of CIS films has been thoroughly investigated. So far, the influence of deposition time [17], concentration of precursors [21], applied potential [22], and complexing agents [2] has been studied. However, the effect of supporting electrolyte concentration on one-step electrodeposited CIS film properties has so far not been addressed.

Supporting electrolytes are normally used during electrodeposition of a film to increase the conductivity of the solution and to keep the ionic strength and pH constant [23]. It has been shown that increasing the concentration of the supporting electrolyte leads to an increase in the values of minimum activation resistance of the electrode reaction and a decrease in the standard rate constants of the first electroreduction step [24]. Accordingly, film properties can be affected and modified by varying the supporting electrolyte concentration. The use of supporting electrolytes has been widely reported for the one-step electrodeposition process because it favors co-deposition [25]. Chloride- and sulfate-based electrolytes are the most used for electrodeposition [2, 25–27]; however, in acidic conditions, sulfate-based electrolytes are not sufficiently inert, resulting in reduction to $SO_{2(g)}$. Therefore, LiCl has been widely used as a support electrolyte in one-step electrodeposited CIS films [2, 19, 28, 29].

In this work, CIS films are fabricated through a one-step electrodeposition method. The effect of the supporting electrolyte concentration on the morphological characteristics, chemical composition, and the optical and structural properties of the CIS films are analyzed. Furthermore, ZnS/CIS bilayers are fabricated using the one-step electrodeposited CIS films, in order to investigate their ability as absorbent layers in TFSCs. The morphological characteristics, chemical composition, and photovoltaic response of the bilayers are reported.

Experimental

Polarization curves and electrodeposition of CIS

Prior to the deposition process, in order to investigate the effect of the supporting electrolyte concentration on the reduction potential of CIS, potentiodynamic measurements were performed. An AMEL 2549 potentiostat/galvanostat in a three-electrode cell configuration was used. A molybdenum (Mo) foil with an exposure surface of 0.5 cm × 0.5 cm, a platinum wire, and a saturated calomel electrode (SCE) were used as the working, counter, and reference electrodes, respectively. Mo substrates (Sigma-Aldrich, 99%, 0.1 mm thick) were cleaned with soap and rinsed with distilled water and alcohol. Subsequently, the Mo substrate was dried at room temperature.

The electrolytic bath contained 7.8 mmol $CuCl_2$, 6.25 mmol $InCl_3$, 23 mmol $C_8H_5KO_4$ (KHP), 23.4 mmol $Na_2S_2O_3$, and X mmol LiCl (X = 50, 100, 150, 200, or 250). The metallic sources, complexing agent, and source of the sulfur ions were kept constant, while the LiCl concentration added to the electrolytic bath was changed, resulting in five different electrolytic baths. The pH was adjusted to 2.5 by adding diluted HCl and the bath temperature was kept constant at 30 °C. The electrolytic bath was deaerated with N_2 gas for 20 min to remove any dissolved oxygen in the solution. The potentiodynamic curves were scanned from 0 to − 1.8 V vs. SCE with a constant scan rate of 10 mV s^{-1}. Polarization curves for each individual ionic species were also performed. It should be noticed that the characteristics found through these analyses are similar to those reported elsewhere [2] and for this reason are not shown here.

The electrodeposition process for CIS thin films was carried out potentiostatically following the same experimental details than those followed for the polarization curves. The one-step electrodeposition process was started by applying a constant potential of − 1 V vs. SCE for 30 min. Then, the electrodeposited samples were removed from the solution and cleaned with distilled water to remove any non-well-adhered material and dried at room temperature. All the obtained CIS thin films were uniformly dark and well covered the surface substrate. The as-deposited samples were labeled as CIS–X, where X = 50, 100, 150, 200, or 250 mmol, which represented the LiCl concentrations added to the electrolytic

Q3 **Fig. 1** Schematic representation of the fabrication of ZnS/CIS/Mo solar cells

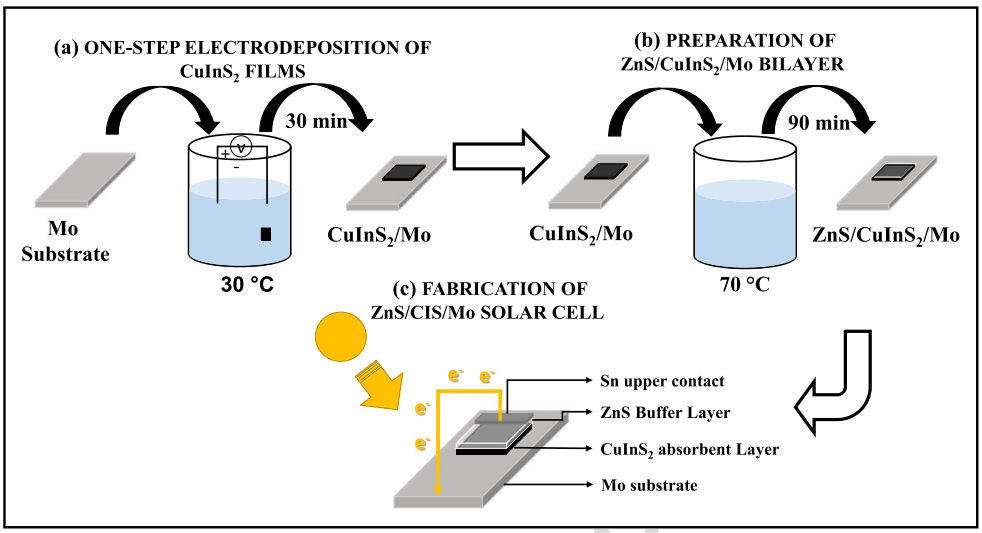

bath, respectively. Finally, the deposited films were annealed in a 95% N_2 + 5% H_2 atmosphere for 1 h at 400 °C. Before heating, air was purged for 90 min and then the program was started with a heating rate of 10 °C/min. The annealed samples were labeled by adding the letter "a" to the previously defined labels (a–CIS–*X*).

For all the as-deposited samples, the morphological characteristics and chemical composition were investigated by scanning electron microscopy (SEM; Hitachi Su 70) coupled with energy-dispersive spectroscopy (EDS). The film thickness was measured using a Bruker Stylus profiler model (Dektak XT). The optical properties were studied by means of diffuse reflectance spectroscopy using an ultraviolet-visible spectrophotometer (Thermo Scientific Evolution 220) with an integrating sphere for solid samples. The band gap values were estimated at the wavelength where a sharp increase in reflectance was observed [30]. After the annealing process of the CIS films, the measurements of the surface characteristics, EDS, and optical band gap were carried out again. In addition, the structural properties were measured by means of X-ray diffraction (XRD) using a D5000 Bruker diffractometer with Cu Kα radiation at 40 kV and 40 mA.

ZnS/CIS heterojunction

In order to investigate the ability of the one-step electrodeposited CIS films as absorbent materials in solar cells, three different ZnS/CIS bilayers are fabricated. A schematic representation of the fabrication of the ZnS/CIS/Mo solar cells is shown in Fig. 1. For construction of the solar cells, the ZnS thin film was chemically deposited on the obtained CIS layer. This was done after electrodeposition of CIS on the Mo substrate (see Fig. 1a). The solution for depositing the ZnS thin film has been reported elsewhere [31]. Once the non-toxic solution was prepared and the pH adjusted to 10.5 (total volume of 100 mL), CIS/Mo substrates were immersed in the reactor (see Fig. 1b). Subsequently, the reactor was transferred to a thermoregulated bath for 90 min at 75 °C. After this time, samples were removed from the solution, rinsed with deionized water, and dried at room temperature. The upper Sn contact was made using a hot ultrasonic soldering unit model (Sunbonder USM-5 from Kuroda Techno Co., Ltd.) (see Fig. 1c).

The morphological characteristics of the obtained ZnS/CIS bilayers were investigated by field emission SEM (MERLIN^{TM}, Carl Zeiss). The semiquantitative chemical composition was measured by EDS combined with SEM. Finally, the photovoltaic response was measured using a solar simulator (Abet Technologies model 10500) as an irradiating source at 1 sun of irradiating power (1 sun = 1000 W/m^2) and a 2401 Source Meter Instrument (Keithley). A silicon reference cell equipped with a KG5 filter was used.

Results and discussion

Cathodic polarization curves

In order to study the effect of the concentration of LiCl on the reduction process of ions to form CIS, cathodic polarization curves were measured. Figure 2 shows the cathodic polarization curves for electrolytic baths with different concentrations of LiCl as a supporting electrolyte. The solution pH was adjusted to 2.5 by adding appropriate amounts of HCl. KHP was used as an effective complexing agent to bring the reduction potentials of Cu^{2+} and In^{+} closer [2]. Cathodic polarization curves for each ionic species were not included here because they can be found elsewhere [2].

In Fig. 2, it can be seen that the polarization curves exhibit a similar behavior for all the different LiCl concentrations.

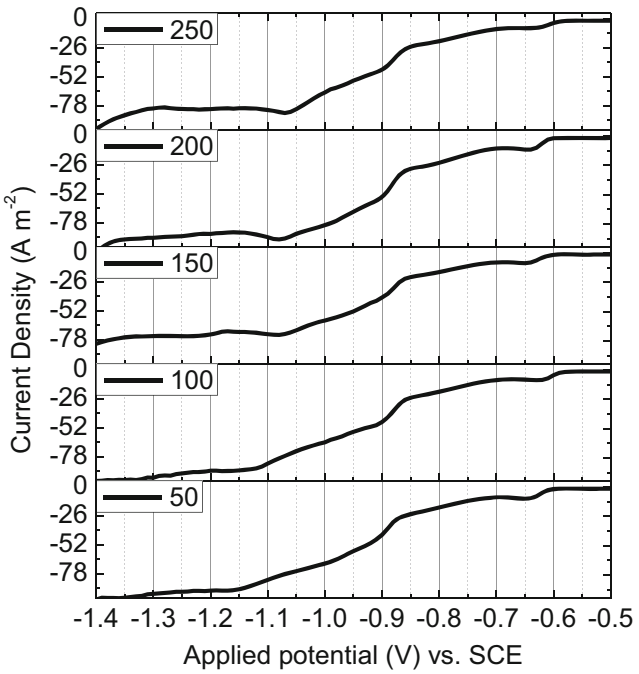

Fig. 2 Cathodic polarization curve for the Cu^{2+} + In^{3+} + KHP + $S_2O_3^{2-}$ + LiCl systems at different concentrations of the supporting electrolyte (pH = 2.5)

Three clear reduction peaks can be observed, which are located at − 0.62, − 0.90, and − 1.1 V vs. SCE. The first peak is attributed to the reduction of Cu^{2+} to Cu^{+} and In^{3+} to In^{+} [2, 21]. The second one is ascribed to the reduction of In^{+} to In^{0} [2], and the last one corresponds to the formation of $Cu_xIn_yS_z$ species (due to the reduction of Cu^{+} to Cu^{0} and In^{+} to In^{0}) [2].

In addition, the slight drop in the current density between − 0.70 and − 0.85 V vs. SCE can be attributed to the reduction of $S_2O_3^{2-}$ to S^0 and S^0 to S^{2-} [2, 21].

Concerning the effect of the LiCl concentration, it can be clearly seen that as the LiCl concentration increases from 50 to 250 mmol, the reduction potential for the formation of $Cu_xIn_yS_z$ species shifts to more positive potentials, namely, from − 1.17 to − 1.05 V vs. SCE. Nieszporek et al. suggested that the easier reduction of ionic species, as the supporting electrolyte concentration increases, is caused by a diminution of the hydration level of metallic ions, as well as the number of water molecules at the electrode surface [24]. In addition, it was experimentally observed that for potentials more negative than −1 V vs. SCE, films are shown to be inhomogeneous, which happened even for slightly more negative potentials (such as − 1.05 V vs. SCE). Hence, the applied potential to deposit the CIS film was chosen to be − 1 V vs. SCE.

Characterization of the as-deposited samples

As-deposited CIS samples were first characterized by SEM and EDS. The films with appropriate morphology and close to the stoichiometric composition were selected to be used as an absorbent layer in solar cells. Figure 3 shows the SEM images for as-deposited CIS films grown at different concentrations of LiCl. The films exhibit a dense and uniform surface with well-defined particles. It can be also observed that the morphology of the CIS samples is affected by the concentration of the supporting electrolyte. For the CIS–50 sample, irregular-shaped particles with agglomerates of ~ 1 μm are

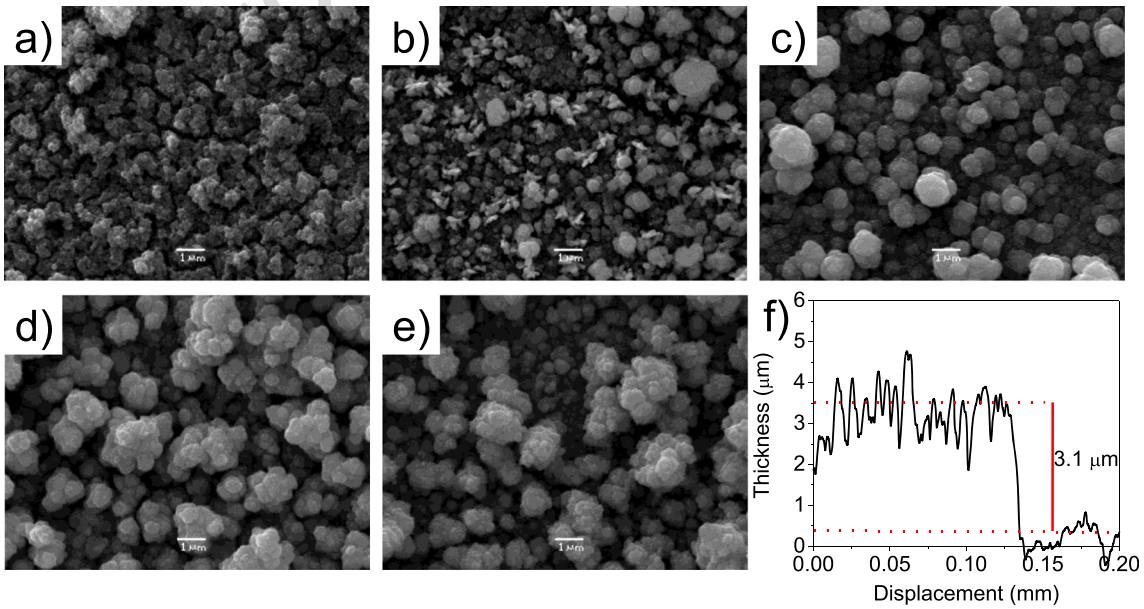

Fig. 3 SEM images for as-deposited samples grown with a 50 mM, b 100 mM, c 150 mM, d 200 mM, and e 250 mM of LiCl. f Profilometric scan of the as-deposited CIS–100 sample

Q4 t1.1 **Table 1** Semiquantitative chemical composition from EDS of the as-deposited samples

t1.2 Sample	Cu (at.%)	In (at.%)	S (at.%)	Cu/In	S/(Cu + In)
t1.3 CIS–250	27.02	26.29	46.51	1.03	0.872
t1.4 CIS–200	29.65	27.04	43.31	1.10	0.763
t1.5 CIS–150	26.90	27.29	45.81	0.99	0.845
t1.6 CIS–100	27.73	32.14	40.13	0.86	0.670
t1.7 CIS–50	19.63	33.73	46.63	0.58	0.873

observed. A noticeable change in morphology is observed for the CIS–100 sample, where a compact layer is obtained and agglomerates with larger sizes are observed (up to 2 μm). These agglomerates tend to grow up to ~ 3.5–4.0 μm as the concentration of LiCl increases from 150 to 250 mmol, respectively. The presence of agglomerates in the surface of electrodeposited CIS films has been reported previously [2, 21]. Additionally, the measured thickness for all obtained CIS films was 2–3 μm (see Fig. 3f) and no clear trend was observed as a function of the LiCl concentration.

Table 1 shows EDS results for the as-deposited samples, where it is clear that the composition for the CIS–50 sample is quite far from the stoichiometric ratio, and a high atomic concentration of In and S was obtained. This is because the

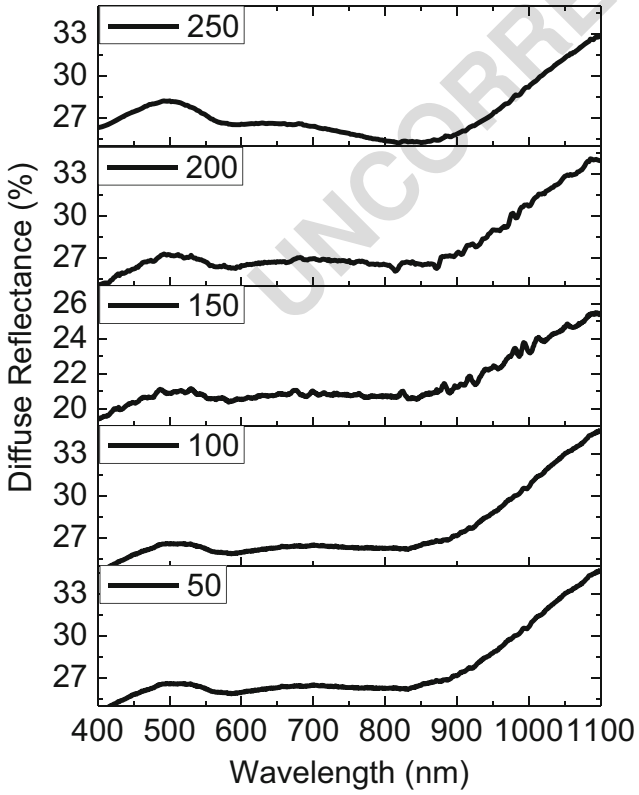

Fig. 4 DRS spectra of the as-electrodeposited CIS samples for different LiCl concentrations

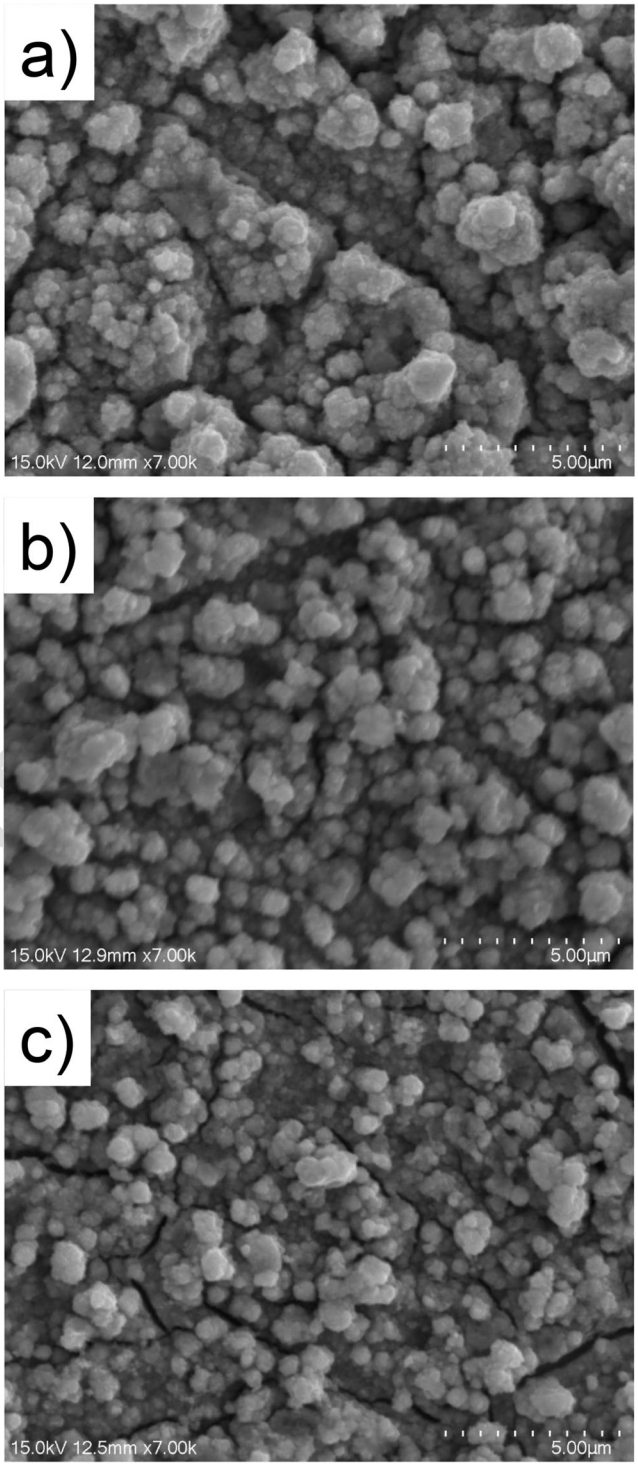

Fig. 5 SEM images for annealed $CuInS_2$ grown with a 150 mM, b 200 mM, and c 250 mM of LiCl

reduction potential for the $Cu_xIn_yS_z$ species with 50 mmol LiCl was less negative than − 1 V vs. SCE (see Fig. 1), resulting in a favorable deposition of In_xS_y on the Mo surface.

For CIS–100, the atomic concentration of Cu increased as a result of the shift to a less negative reduction potential for $Cu_xIn_yS_z$ species. For the other samples, the Cu/In ratio was

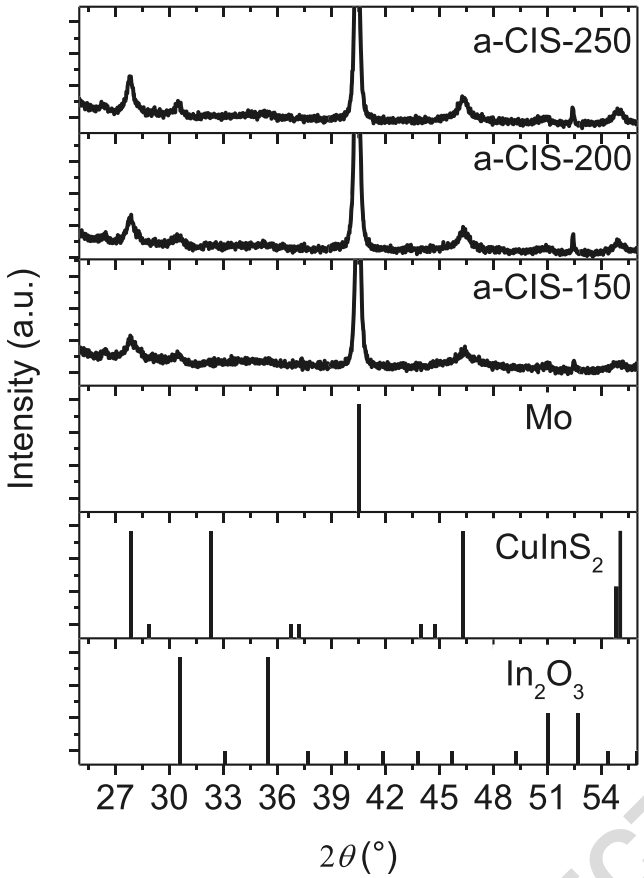

Fig. 6 Diffractograms for annealed $CuInS_2$ films

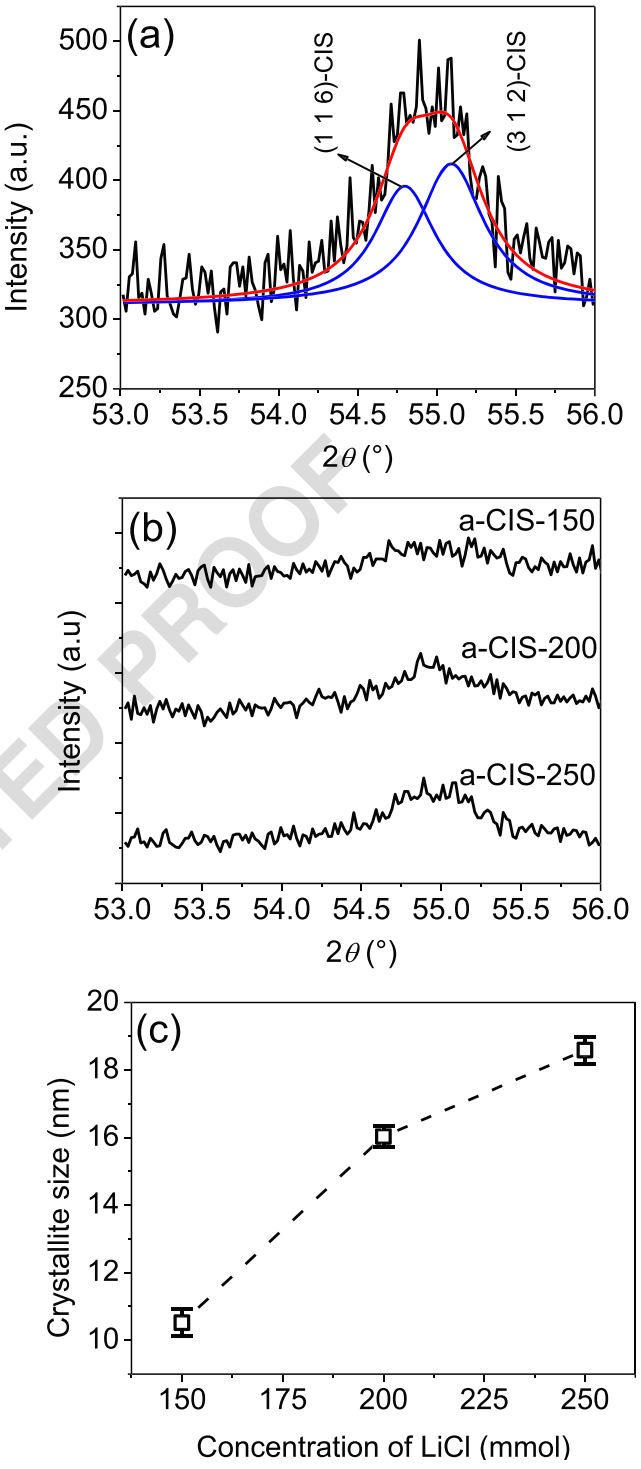

Fig. 7 a Deconvolution of XRD peaks corresponding to (1 1 6) and (3 1 2) planes, b close-up of the XRD patterns between angles 53 and 56°, and c crystallite size for annealed $CuInS_2$ films

closer to the stoichiometric composition for CIS (i.e., 1); however, a slightly lower atomic concentration of S was obtained, where S/(Cu + In) was always below 1. The lower sulfur content in the one-step electrodeposited CIS films has also been reported previously [9].

Figure 4 shows the diffuse reflectance spectra of the as-deposited CIS films obtained at different concentrations of LiCl. From the spectra, a sharp increase in diffuse reflectance at wavelengths above 850 nm can be observed, which agrees well with the absorption edge of the CIS films. As shown in Fig. 4, the edge is shifted from 876 to 894 nm as the concentration of the supporting electrolyte increases. This leads to a slight reduction in the band gap values from 1.41 to 1.38 eV, all of which are in good agreement with those reported previously for CIS films [32, 33].

From the above characterization, it can be observed that the optical properties of the obtained films are not strongly affected by the LiCl concentration; however, CIS–150, CIS–200, and CIS–250 are closer to the expected stoichiometric Cu/In and S/(Cu + In) ratios. Furthermore, the as-deposited samples did not show any peaks in their XRD patterns (not shown here), confirming the amorphous nature of the as-deposited samples. For applications in solar cells, annealing is normally performed to crystallize electrodeposited CIS films, which will improve the electron mobility and charge transport and reduce recombination at the interface between the absorbent and the buffer layer.

In this sense, CIS–150, CIS–200, and CIS–250 samples are the most suitable to be used as absorbent layers in solar cells (composition close to the stoichiometric one), and therefore, only these samples were subjected to annealing.

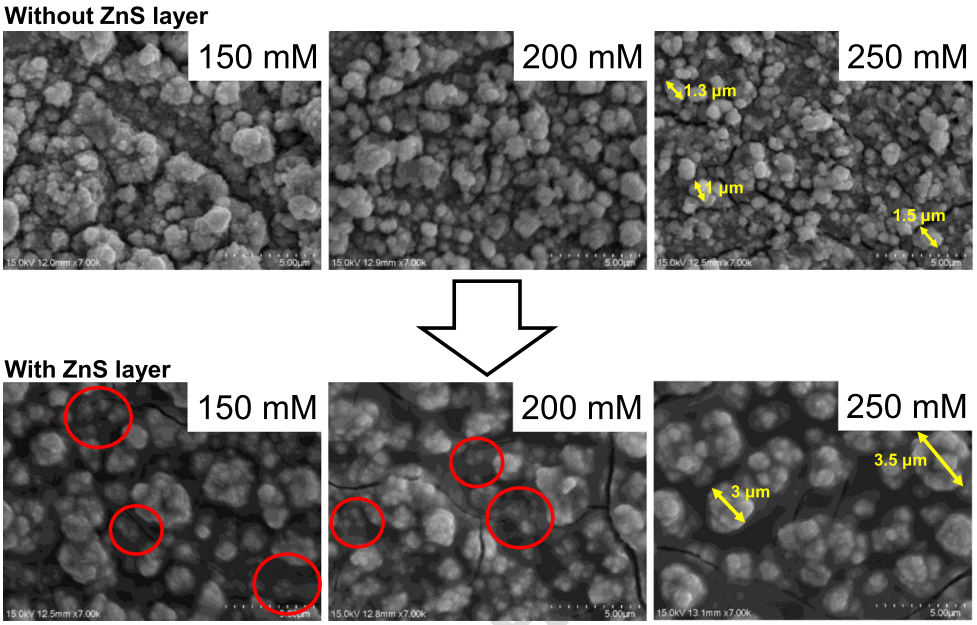

Fig. 8 Surface view of the annealed $CuInS_2$ samples without and with a ZnS layer

Characterization of annealed samples

Figure 5 shows the SEM images for annealed samples (a–CIS–150, a–CIS–200, and a–CIS–250). In this figure, a decreased size of aggregates can be observed when compared with the as-deposited samples (see Fig. 3), with sizes in the range of 1–2 µm. Since electrodeposition is a non-equilibrium technique used to obtain films, the decreasing size of aggregates could be a consequence of the surface diffusion and crystallization during the annealing process. It was also observed that the particle size tends to decrease as the LiCl concentration increases. This characteristic indicates that as the LiCl concentration increases, the non-equilibrium conditions for CIS deposition augment. This results in unstable and larger size agglomerates, which decrease in size after annealing. To explain this, we considered the CIS–250 sample as an example: the as-deposited sample showed the largest size of agglomerates (Fig. 3e) and after annealing showed the lowest size of agglomerates (Fig. 5c). In addition, for all the annealed samples, some cracks were also seen, which can be attributed to residual stresses from the electrodeposition process.

The band gap values of the annealed samples were found to be between 1.42 and 1.49 eV, with no clear relation observed as a function of LiCl concentration. After annealing, a slight increase in the average band gap was observed, which could be attributed to the appearance of the In_2O_3 phase discussed below (the band gap for In_2O_3 can be found between 3.0 and 3.5 eV [34, 35]). It has been previously reported that the presence of secondary phases with wider band gaps leads to a slight increase in the CIS band gap [36].

Figure 6 displays the XRD patterns for the annealed CIS samples. For all films, a strong peak located at $2\theta = 40.5°$ was observed, which is ascribed to the (1 1 0) plane of the cubic phase of Mo (Powder Diffraction File (PDF) N° 04–0809). Two other peaks are identified located, which are located at $2\theta = 27.87°$ and 46.31°. These peaks are attributed to the reflection of the (1 1 2) and (2 0 4) planes of the tetragonal phase of CIS according to PDF N° 32–0339. Another peak close to $2\theta = 55°$ can be observed, which is due to the contribution of two different peaks located at 54.73° and 55.09° ascribed to the (1 1 6) and (3 1 2) planes, respectively, of the tetragonal phase of CIS (see Fig. 7a). There are also two weak peaks positioned at $2\theta = 30.48°$ and 52.76°, which correspond to the (2 2 2) and (4 3 3) planes of the cubic In_2O_3 phase, respectively. The presence of secondary phases in electrodeposited CIS films has been previously reported and is a consequence of the annealing process [3, 20].

A detailed inspection of the diffractograms revealed a reduction in the intensity of the peaks as the concentration of LiCl decreased. This can clearly be seen in Fig. 7b, where a reduction

Table 2 EDS results for annealed CIS samples and ZnS/CIS heterojunctions (metal = Zn + Cu + In, Zn = 0 for samples a–CIS–250, a–CIS–200, and a–CIS–150)

Sample	Zn (at.%)	Cu (at.%)	In (at.%)	S (at.%)	Cu/In	Sulfur/metal
ZnS/CIS–250	3.20	25.82	21.16	49.83	1.22	0.993
ZnS/CIS–200	1.16	25.79	25.89	47.21	0.996	0.893
ZnS/ CIS–150	5.22	23.06	24.82	46.90	0.929	0.883

JmlID 10008_ArtID 4622_Proof# 1 - 18/05/2020

in the intensity of the (1 1 6) and (3 1 2) planes of the CIS phase as the LiCl concentration increases is observed. In order to estimate the crystallite size for the CIS phase, the Williamson-Hall analysis was carried out [37]. Figure 7c shows the crystallite size as a function of the LiCl concentration, where an increase in the crystal size is indicated. The supporting electrolyte has a direct impact on the electrolytic bath conductivity, i.e., the higher the LiCl concentration, the greater the conductivity (and current density). It is known that in electrodeposition, the deposited mass is directly proportional to the current density. Therefore, as the LiCl concentration increases, a greater mass is deposited for the same deposition time. Thus, higher LiCl concentrations lead to morphological disorder that causes an increase in crystallite size after the annealing process.

ZnS/CIS bilayers for solar cell applications

The annealed CIS samples were used to fabricate bilayers for potential application in TFSC devices. Figure 8 shows the surface of the CIS films without and with the ZnS thin-film layer. A change in the surface characteristics is clearly observed when the ZnS thin film is deposited on the surface of the CIS films. The ZnS thin film covers the surface of the CIS layer, especially between the particles and aggregates (see red highlighted circles). Additionally, for all the obtained bilayers, it can also be seen that ZnS deposition leads to an increase in the aggregate size. This can be clearly seen in the a–CIS–250 sample, where aggregate sizes increased from 1.0–1.5 μm (before ZnS deposition) to 3.0–3.5 μm (after ZnS deposition). This could be due to a higher growth rate of aggregates and larger particles, which act as preferential nucleation sites.

When comparing the surface characteristics of the three ZnS/CIS bilayers, it is possible to observe that the amount of aggregates tends to decrease for higher LiCl concentrations. This could be associated with the decrease in particle size of the annealed CIS samples, as the LiCl concentration increases. Additionally, some cracks can be seen that could be related to the deposition rate that induces stress at the interface between ZnS and CIS [38].

The EDS analysis for the ZnS/CIS bilayers, summarized in Table 2, reveals the presence of small amounts of Zn, which is consistent with the expected film thickness (lower than 100 nm). No significant changes in the Cu/In and S/metal ratios were observed after the ZnS film deposition.

Concerning the ability of one-step electrodeposited CIS as an absorber layer in solar cells, the photovoltaic response of the ZnS/CIS bilayers was measured by recording the *J*–*V* curve under simulated solar radiation. Figure 9 shows the *J*–*V* curve for the ZnS/a–CIS–250 bilayer, which was the only sample that exhibited a photovoltaic response. This could be a consequence of the surface characteristics of annealed CIS samples and the low growth rates for ZnS thin films deposited from non-toxic solutions [39]. The particle size of the a–CIS–250 sample is

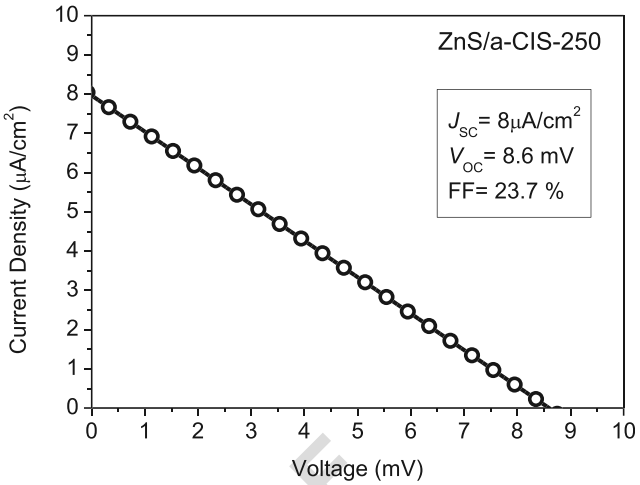

Fig. 9 Current density-voltage (J–V) curve of the ZnS/a–CIS–250 sample

lower; this could lead to better coverage of ZnS and therefore the formation of a homogeneous bilayer. In this sense, further studies need to be carried out to find the experimental conditions that result in better coverage of ZnS on the CIS surface. For instance, in the present work, deposition of ZnS thin films was performed at 75 °C and it was observed that deposition times higher than 90 min were impractical because of solution evaporation. Therefore, different paths could be evaluated to solve this issue, such as changes in reactant concentration, solution pH, or deposition of ZnS in several layers (to increase the ZnS film thickness and coverage).

From Fig. 9, it can be seen that the best values for the photocurrent (J_{sc}) and open-circuit potential (V_{oc}) were quite low (J_{sc} below 10 μA/cm^2 and V_{oc} of 8.6 mV). The best fill factor value reached was 23.7% and the efficiency of the device was lower than 1%. The linear-like behavior shown in the *J*–*V* curve may be observed for solar cells with lower values of FF and efficiency [40, 41]. As for the low efficiency reported in the present article, it is likely the result of several factors; for example, the presence of cracks on the surface has been reported as a detrimental characteristic in solar cells that reduces the J_{sc} in solar cells [42, 43]. In addition, the low fill factor value indicates that there is still a need to optimize the device manufacturing process. In spite of the low photovoltaic response of the ZnS/CIS bilayer obtained, it was shown that ZnS/CIS is a heterojunction that can convert solar energy into electricity. It should be noted that this was the first attempt to obtain a ZnS/CIS heterojunction, where the ZnS film was deposited by a non-toxic chemical solution and the CIS layer was grown using one-step electrodeposition.

Conclusions

CIS thin films with a chemical composition close to the stoichiometric one were obtained in this work using a one-step

electrodeposition process. The effect of different LiCl concentrations as a supporting electrolyte was investigated and it can be concluded that higher concentrations of LiCl resulted in larger agglomerates of CIS and a Cu:In:S ratio close to the stoichiometric composition for CIS films. After the annealing process, a reduction in the agglomerate size and a decrease in particle size as the supporting electrolyte concentration increased were observed. Regarding the structural properties after annealing, larger crystallite sizes were obtained because of the disorder as the LiCl concentration increased. Concerning the ZnS/CIS bilayer, it can be concluded that ZnS better covers the surface of the a–CIS–250 sample due to the smaller particle size. From photovoltaic characterization, it was shown that the bilayer system composed of a ZnS buffer layer synthesized by a non-toxic solution and a CIS absorbent layer prepared by one-step electrodeposition with a LiCl concentration of 250 mmol has potential for thin-film solar cell applications.

Acknowledgments The authors acknowledge the use of Servicio General de Apoyo a la Investigación–SAI, Universidad de Zaragoza, Spain.

Funding information This work was financially supported by the *Comisión Nacional de Ciencia y Tecnología* (CONICYT) through the project FONDECYT Iniciación 11160368 and Gobierno de Aragón–Fondo Social Europeo (E14 17R).

Data availability All data generated or analyzed during this study are included in this published article. Other datasets generated and/or analyzed during the current study are available from the corresponding author on reasonable request.

Compliance with ethical standards

Conflict of interest The authors declare that they have no conflict of interest.

Code availability Not applicable.

References

1. Störkel U, Argour M, Murrell C, Lewerenz H (2001) Electrochemical treatment of $CuInS_2$. Thin Solid Films 387(1-2): 182–184
2. Xu X, Wang F, Liu J, Ji J (2010) Effect of potassium hydrogen phthalate ($C_8H_5KO_4$) on the one–step electrodeposition of single-phase $CuInS_2$ thin films from acidic solution. Electrochim Acta 55(15):4428–4435
3. Tang Y, Ng Y, Yun J, Amal R (2014) Fabrication of a $CuInS_2$ photoelectrode using a single-step electrodeposition with controlled calcination atmosphere. Roy Soc Ch Adv 4:3278
4. Moreau A, Insignares C, Escoubas L, Simon J, Bermúdez V, Pérez A, Izquierdo V, Ruiz C (2015) Impact of Cu-Au type domains in high current density $CuInS_2$ Solar cells. Sol Energ Mat Sol C 139: 101–107
5. Guo J, Chang G, Zhang W, Liu X, He Y (2016) Facile synthesis of $CuInS_2$ nanoparticles using different alcohol amines as solvent. Chem Phys Lett 647:51–54
6. Abushama J, Rommel N, Johnston S, Ward S, Wu X (2005) Improved performance in $CuInSe_2$ and surface–modified $CuGaSe_2$ solar cells. Proceedings of the 31st IEEE Photovoltaic Specialists Conference, Lake Buena Vista, 299–302.
7. Green M, Hishikawa Y, Dunlop E, Levi D, Hohl J, Ho A (2018) Solar cell efficiency tables (version 51). Prog Photovolt 26(1):3–12
8. Goto H, Hashimoto Y, Ito K (2004) Efficient thin film solar cell consisting of TCO/CdS/$CuInS_2$/$CuGaS_2$ structure. Thin Solid Films 451–452:552–555
9. Nakabayashi T, Miyazawa T, Hashimoto Y, Ito K (1997) Over 10 % efficient $CuInS_2$ solar cell by sulfurization. Sol Energ Mat Sol C 49(1-4):375–381
10. Yuan J, Shao C, Zheng L, Fan M, Lu H, Hao C, Tao D (2014) Fabrication of $CuInS_2$ thin film by electrodeposition of Cu–In alloy. Vacuum 99:196–203
11. Zhuang M, Wei A, Zhao Y, Liu J, Yan Z, Liu Z (2015) Morphology controlled growth of special nanostructure $CuInS_2$ thin films on an FTO substrate and their application in thin film solar cells. Int J Hydrogen Energ 40(1):806–814
12. Peng S, Liang J, Zhang L, Shi Y, Chen J (2007) Shape–controlled synthesis and optical characterization of chalcopyrite $CuInS_2$ microstructures. J Cryst Growth 305(1):99–103
13. Bollero A, Trigo J, Herrero J, Gutiérrez M (2009) Simplified modulated evaporation process for production of $CuInS_2$ films with reduced substrate temperatures. Thin Solid Films 517(7):2167–2170
14. Cherian A, Jinesh K, Kashiwaba Y, Abe T, Balamurugan A, Dash S, Tyagi A, Kartha C, Vijayakumar K (2012) Double layer $CuInS_2$ absorber using spray pyrolysis: a better candidate for CuInS2/In2S3 thin film solar cells. Sol Energy 86(6):1872–1879
15. Di Iorio Y, Vázquez M (2017) Inexpensive methodology to prepare TiO_2/$CuInS_2$ hetero–junctions for photovoltaic applications. Mater Res Express 4(4):045903
16. Broussillou C, Andrieux M, Herbst M, Jeandin M, Jaime J, Morin S (2011) Sulfurization of Cu–In electrodeposited precursors for $CuInS_2$–based solar cells. Sol Energ Mat Sol C 95:S13–S17
17. Lu L, Wang Y, Li V (2012) Influence of processing parameters on the preparation of $CuInS_2$ thin film by one–step electrodeposition as the solar cell absorber. Surf Coat Technol 212:55–60
18. Greenwood N, Earnshaw A (1997) Chemistry of the elements (2nd ed.). Butterworth-Heinemann. ISBN 0–08–037941–9.
19. Martínez A, Fernández A, Arriaga L, Cano U (2006) Preparation and characterization of Cu–In–S thin films by electrodeposition. Mater Chem Phys 95(2-3):270–274
20. Asenjo B, Chaparro M, Gutiérrez M, Herrero J (2006) Electrochemical growth and properties of $CuInS_2$ thin films for solar energy conversion. Thin Solid Films 511–512:117–120
21. Cheng K, Chiang W (2011) Effect of [Cu]/[Cu+In] ratio in the solution bath on the growth and physical properties of $CuInS_2$ films using one–step electrodeposition. J Electroanal Chem 661(1):57–65
22. Guan R, Cao L, Sun Q, Cao Y (2015) Effects of preparation conditions on the $CuInS_2$ films prepared by one–step electrodeposition method. J Nanomater 2015:ID678929
23. Wang J (2006) Analytical Electrochemistry, 3rd edn. Wiley, USA
24. Nieszporek J, Gugala D, Nieszporek K (2019) The effect of supporting electrolyte concentration on zinc electrodeposition kinetics from methimazole solutions. Electroanalysis 31(6):1141–1149
25. Dhanwate V, Chaure N (2013) Effect of growth potential on the electrodeposition of CIS thin films. Appl Nanosci 2:1–5
26. Ribeaucourt L, Savidant G, Lincot D, Chassaing E (2011) Electrochemical study of one–step electrodeposition of copper-indium-gallium-alloys in acidic condition as precursors layers for Cu(In,Ga)Se_2 thin films solar cells. Electrochim Acta 56(19):6628–6637

27. You R, Lew K, Fu Y (2014) Effect of electrodeposition potential on composition of $CuIn_{1-x}Ga_xSe_2$ absorber layer for solar cell by one–step electrodeposition. Int J Photoenergy 2014:478428
28. Martínez A, Arriaga L, Fernandez A, Cano U (2004) Band edge determination of $CuInS_2$ thin films prepared by electrodeposition. Mater Chem Phys 88:41–420
29. Xu X, Wang F, Liu J, Park K, Fujishig M (2011) A novel one–step electrodeposition to prepare single–phase $CuInS_2$ thin films for solar cells. Sol Energy Mater Sol Cells 95(2):791–796
30. Wijesundera R, Siripala W (2004) Preparation of $CuInS_2$ thin films by electrodeposition and sulphurization for applications in solar cells. Sol Energy Mater Sol C 81(2):147–154
31. Rodríguez C, Sandoval M, Cabello G, Flores M, Fernández H, Carrasco C (2014) Characterization of ZnS thin films synthesized through a non–toxic precursors chemical bath. Mater Res Bull 60: 313–321
32. Di Iorio Y, Berruet M, Schreiner W, Vázquez M (2014) Characterization of $CuInS_2$ thin films prepared by one–step electrodeposition. J Appl Electrochem 44(12):1279–1287
33. Rabeh M, Khedmi N, Fodha M, Kanzari M (2014) The effect of thickness on optical band gap and N-type conductivity of $CuInS_2$ thin films annealed in air atmosphere. Energy Procedia 44:52–60
34. Sharma R, Mane R, Mn S, Han S (2009) Optimization of growth of In_2O_3 nano-spheres films by electrodeposition for dye-sensitized solar cells. J Alloys Compd 479(1-2):840–843
35. Henriquez R, Muñoz E, Dalchiele E, Marotti R, Martin F, Leinen D, Ramos J (2013) Electrodeposition of In_2O_3 thin films from dimethyl sulfoxide based electrolytic solution. Phys Status Solidi A 210(2):297–305
36. Liang W, Yanlai W, Wei Y, Jun Z, Jiangang X (2015) Effect of sulfurization time on the formation of $CuInS_2$ thin films. Rare Metal Mater Eng 44(4):805–807
37. Rodríguez C, Sandoval M, Saavedra R, Trejo C, De la Carrera F, Aragón L, Sirena M, Delplancke M, Carrasco C (2016) Comprehensive study of growth mechanism and properties of low Zn content $Cd_{1-x}Zn_xS$ thin films by chemical bath. Mater Res-Ibero-Am J 19:1335–1343
38. Hong J, Lim D, Eo Y, Choi C (2017) Chemical bath deposited ZnS buffer layer for $Cu(In,Ga)Se_2$ thin films solar cell. Appl Surf Sci 432:250–254
39. Agawane G, Shin S, Kim M, Suryawanshi M, Gurav K, Moholkar A, Lee J, Yun J, Patil P, Kim J (2013) Green route fast synthesis and characterization of chemical bath deposited nanocrystalline ZnS buffer layers. Curr Appl Phys 13(5):850–856
40. Valdés M, Berruet M, Goosens A, Vázquez M (2010) Spray deposition of $CuInS_2$ on electrodeposited ZnO for low-cost solar cells. Surf Coat Technol 204(24):3995–4000
41. Dehghani M, Behjat A, Tajabadi F, Taghavinia N (2015) Totally solution-processed $CuInS_2$ solar cells based on chloride inks: reduced metastable phased and improved current density. J Phys D Appl Phys 48(11):115304
42. Dhimish M, Holmes V, Mehrdadi B, Dales M (2017) The impact of cracks on the photovoltaic power performance. J Sci Adv Mater Devices 2:199–2009
43. Ennemri E, Logerais P, Balistrou M, Durastanti J, Belaidi I (2019) Cracks in silicon photovoltaic modules: a review. J Optoelectron Adv Mater 21:74–92

AUTHOR QUERIES

AUTHOR PLEASE ANSWER ALL QUERIES.

Q1. Please check if the corresponding author's affiliation and email address are correctly captured/ indicated. Also, please check if the author names and affiliations are presented correctly.
Q2. Please check if keywords are captured and presented correctly.
Q3. Please check if figure captions and their corresponding images are captured and presented correctly.
Q4. Please check if all the tables are presented correctly.